Microbial electrosynthesis from CO_2 reaches productivity of syngas and chain elongation fermentations

Cabau-Peinado, Oriol; Winkelhorst, Marijn; Stroek, Rozanne; de Kat Angelino, Roderick; Straathof, Adrie J.J.; Masania, Kunal; Daran, Jean Marc; Jourdin, Ludovic

DOI
10.1016/j.tibtech.2024.06.005

Publication date
2024

Document Version
Final published version

Published in
Trends in Biotechnology

Trends in Biotechnology

CellPress OPEN ACCESS

Research Article

Microbial electrosynthesis from CO_2 reaches productivity of syngas and chain elongation fermentations

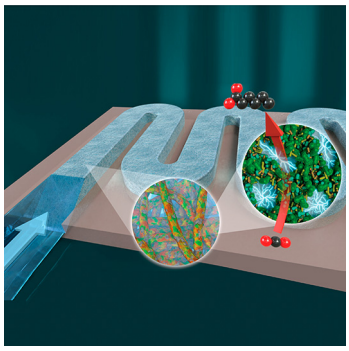

Carbon-based products are crucial to society. However, their production from fossil-based carbon is unsustainable. We developed a scalable microbial electrosynthesis process that produces medium-chain carboxylic acids from CO_2 and renewable electricity, using microorganisms as a catalyst. This represents a promising avenue for generating low CO_2-footprint precursors for the chemical, fuel, feed, and food industries.

Oriol Cabau-Peinado, Marijn Winkelhorst, Rozanne Stroek, Roderick de Kat Angelino, Adrie J.J. Straathof, Kunal Masania, Jean Marc Daran, Ludovic Jourdin

L.Jourdin@tudelft.nl (L. Jourdin).

Highlights

Sustainable production of carbon-based products is urgently needed.

A novel directed flow-through microbial electrosynthesis (MES) reactor was designed and characterized for carbon dioxide (CO_2) conversion to C2–C6 carboxylates.

Three-times denser biofilm, volumetric current density, and productivity were achieved compared with the state of the art.

Biomass-specific production rates were maintained over more than 200 days, yet still an order of magnitude lower than that achieved by acetogens in syngas fermentation.

Volumetric productivity in MES was comparable with that from syngas fermentation.

Clostridium luticellarii and *Eubacterium limosum* were the dominant species.

Trends in Biotechnology, November 2024, Vol. 42, No. 11
https://doi.org/10.1016/j.tibtech.2024.06.005

CellPress
OPEN ACCESS

Trends in
Biotechnology

Research Article

Microbial electrosynthesis from CO_2 reaches productivity of syngas and chain elongation fermentations

Oriol Cabau-Peinado[1,3], Marijn Winkelhorst[1], Rozanne Stroek[1], Roderick de Kat Angelino[1], Adrie J.J. Straathof[1], Kunal Masania[2,3,@], Jean Marc Daran[1], and Ludovic Jourdin[1,3,4,*]

Carbon-based products are essential to society, yet producing them from fossil fuels is unsustainable. Microorganisms have the ability to take up electrons from solid electrodes and convert carbon dioxide (CO_2) to valuable carbon-based chemicals. However, higher productivities and energy efficiencies are needed to reach a viability that can make the technology transformative. Here, we show how a biofilm-based microbial porous cathode in a directed flow-through electrochemical system can continuously reduce CO_2 to even-chain C2–C6 carboxylic acids over 248 days. We demonstrate a threefold higher biofilm concentration, volumetric current density, and productivity compared with the state of the art. Most notably, the volumetric productivity (VP) resembles those achieved in laboratory-scale and industrial syngas (CO-H_2-CO_2) fermentation and chain elongation fermentation. This work highlights key design parameters for efficient electricity-driven microbial CO_2 reduction. There is need and room to improve the rates of electrode colonization and microbe-specific kinetics to scale up the technology.

Technology readiness

Microbial electrosynthesis (MES) of carboxylic acids from CO_2 and electricity has been validated for over a decade, now reaching Technology Readiness Levels 3/4 in laboratory settings. However, process optimization is needed before demonstrating an industrial prototype. Key challenges for full-scale implementation include ensuring production stability. Critical areas to investigate and demonstrate are: (i) the impact of CO_2 feed stream composition and properties; (ii) the short- and long-term effects of renewable electricity supply intermittency; and (iii) the flexibility of MES operations and the integrated process, including up- and downstream processes. Moreover, a comprehensive market analysis is required for each target product. For instance, hexanoic acid, which serves as a precursor for nylon, plasticizers, lubricants, pharmaceuticals, fragrances, fuels, and animal feed, necessitates the development of business models that consider complete supply chains and systems.

Introduction

By exploiting the ability of microorganisms to reduce CO_2, **microbial electrosynthesis (MES)** (see Glossary) has become a candidate technology to satisfy the growing demand for fossil-free chemical synthesis, by harnessing the increasing amount of electrical energy obtained from renewable sources [1]. Microbiomes are living systems with the ability to self-repair and regenerate, offering a major advantage for resilient industrial applications over abiotic CO_2 electrolysis. Unlike heterogeneous catalysts, which exhibit stability for limited durations (hours/days), microbial electrochemical reactors demonstrate remarkable operational continuity lasting for several years [2]. Beyond their robustness, biocatalysts in MES systems exhibit the capacity to generate multicarbon products with notable selectivity and **faradaic efficiency** [3]. The bioelectrochemical reduction of CO_2 to produce medium-chain carboxylic acids (MCCAs), such as butyric (four carbons, C4) and caproic (six carbons, C6) acids, presents a promising avenue for generating low CO_2 footprint precursors crucial for applications in the fuel, chemical, feed, and food industries [4,5]. Nonetheless, existing studies elucidating microbial CO_2 reduction to MCCAs report production rates lower than those achieved in alternative fermentation technologies for organics production, including syngas fermentation and chain elongation fermentation [6–9].

Following the initial proof-of-concept demonstrating the production of soluble organics from CO_2 in MES [10], the primary focus within the MES research community has centered on enhancing microbial catalysts, improving cathode materials, and elucidating fundamental mechanisms and microbial functionalities [2,11]. These endeavors have been pivotal in achieving noteworthy

[1]Department of Biotechnology, Delft University of Technology, van der Maasweg 9, 2629, HZ, Delft, The Netherlands
[2]Shaping Matter Lab, Faculty of Aerospace Engineering, Delft University of Technology, Kluyverweg 1, Delft 2629 HS, The Netherlands
[3]LinkedIn: www.linkedin.com/in/oriolcabaupeinado/ (O. Cabau-Peinado), www.linkedin.com/in/kunal-masania-67427914/ (K. Masania); www.linkedin.com/in/ludovic-jourdin-4a726b45/ (L. Jourdin).
[4]Website: www.tudelft.nl/en/faculty-of-applied-sciences/about-faculty/departments/biotechnology/ (L. Jourdin).

 https://doi.org/10.1016/j.tibtech.2024.06.005

*Correspondence:
L.Jourdin@tudelft.nl (L. Jourdin).
@X: @kmasania (K. Masania).

key performance indicators (KPIs), including productivities and faradaic efficiencies. Nevertheless, these KPIs have not yet reached a level that ensures the economic viability of the technology [4,11]. In the context of transitioning to industrial implementation of MES and its potential role in the electrification of the chemical industry, reactor design emerges as a crucial aspect requiring attention [2,11]. State-of-the-art MES reactors capable of producing acids longer than C2 are predominantly **biofilm**-driven systems, exploiting the proximity to the electron source for CO_2 reduction [2,6,12]. Biofilm-driven MESs have so far outperformed MES driven by microorganisms in suspension by several orders of magnitude [3]. Nevertheless, biofilms growing in other environments have demonstrated susceptibility to mass transfer limitations, impacting microbial activities due to the need for substrates and products to diffuse in and out of biofilms [13–16]. Despite these limitations, relatively few efforts have been dedicated to researching and developing biofilm-driven MES reactor design concepts that ameliorate mass transport [6,17,18].

The predominant focus in devising innovative reactor designs has been directed toward MES systems using microorganisms in suspension [19]. Notably, Cui and colleagues recently presented an electrolytic bubble column featuring an external hollow-fiber membrane gas–liquid contactor for the production of acetate from CO_2, achieving an acetate titer and production rate of up to 34.5 g l^{-1} and 1.15 g l^{-1} day^{-1} at an average faradaic efficiency of 64% into acetate [20]. In a different approach, Rosa and coworkers retrofitted a conventional stirred bioreactor with electrodes, showcasing adaptability to MES applications [21,22]. Enzmann and colleagues introduced a bioelectrochemical bubble-column reactor, serving the dual function of a microbial fuel cell and MES system [23]. They tested MES of methane and obtained a mean methane production rate of 36.7 ± 7.8 mmol m^{-2} day^{-1} at a faradaic efficiency of 49.9 ± 4.1%. Puig and coworkers explored a tubular MES reactor for the production of 34.7 mMC of acetate and 87.5 mMC of butyrate at a **current density** of –2.74 ± 0.09 A m^{-2} and faradaic efficiency of ~60% [24]. In another study, they used the same tubular MES for the production of 35–47 mMC of acetate and ethanol at a 1:1 ratio, at a current density of –0.33 to 0.55 A m^{-2} and faradaic efficiency of 12–14% [25]. Additionally, a 4.3-l scaled-up version of a flat-plate double-chamber reactor design demonstrated the production of 3.6 ± 0.6 g l^{-1} acetate at a rate of 0.23 g l^{-1} day^{-1} by microorganisms in suspension, at –6.6 A m^{-2} and a faradaic efficiency of 82% [26].

Configurations for biofilm-driven MES using flow-through designs, where convective flow is intensified near the biofilm–cathode interface, have resulted in elevated production rates, enhanced biofilm growth, and increased carbon selectivity toward longer MCCAs compared with other tested designs [6,13]. However, the flat-plate design used by Jourdin and colleagues presents scalability challenges [6]. In this design, the cathode compartment featured a 1.2 cm-thick free-flowing catholyte volume positioned between the membrane and the 3D-filamentous cathode. The catholyte was directed to flow through the cathode material and exit the compartment on the opposite side, where an additional 1.2 cm-thick free-flowing liquid volume was located. The incorporation of such free-flowing liquid dead-volumes substantially increased both the footprint and capital cost of the reactor upon scale-up. Moreover, these dead-volumes contributed to issues related to hydrogen accumulation, negatively impacting system performance [27]. The fluid dynamics within this reactor design exhibited suboptimal characteristics, leading to dead zones within the cathode material where mass transport and microbial activity were constrained. Furthermore, the 2.4-cm separation between the anode and the cathode proved to be excessively large, resulting in considerable **ohmic drop** and mass transfer resistances, consequently leading to high energy losses [11].

Here, we introduce a directed-flow-through bioelectrochemical reactor (DFBR) featuring a serpentine flow-pattern architecture (Figure 1A,B). In this innovative design, a CO_2-saturated

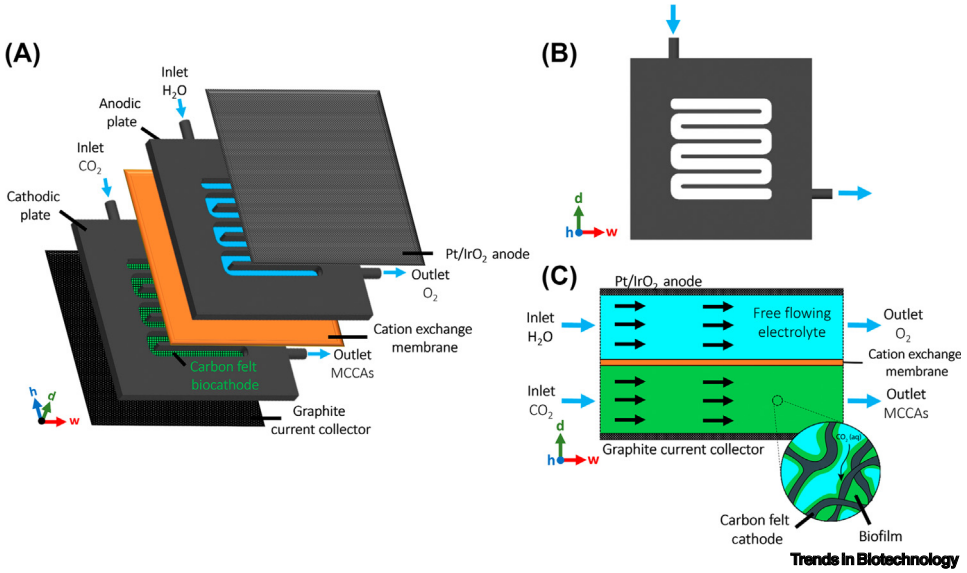

Figure 1. Schematic of a directed-flowthrough serpentine bioelectrochemical reactor. (A) Reactor cell diagram. Each unit comprises a serpentine plate filled with a carbon-based 3D-**biocathode** on a graphite current collector, an empty serpentine plate (free-flowing electrolyte) on a Pt/IrO_2-coated 2D-titanium anode, and a cation exchange membrane. (B) Schematic of the serpentine plate design. (C) Top-view schematic of both flow channels on a reactor cell unit. Abbreviation: MCCAs, medium-chain carboxylic acids.

catholyte is directed through a continuous serpentine channel entirely filled with a porous 3D carbon-based electrode, where CO_2 undergoes biological reduction to form MCCAs (Figure 1C). Unlike previously used systems, the DFBR design eliminates free-flowing liquid in the cathode chamber, thereby facilitating substrate and product turnover at the biofilm–cathode surface. Additionally, the serpentine flow pattern enables an extended residence time, potentially enhancing carbon and electron/hydrogen utilization efficiency, which are key performance indicators upon scale-up. While not explored in this study, the ability to manipulate this residence time theoretically positions this reactor design for further carbon elongation toward carboxylic acids longer than C6. Notably, the design is characterized by its scalability and stackability, enhancing its versatility and applicability.

Serpentine flow channels have been used in many electrochemical systems (e.g., fuel cell, CO_2 electrolysis, etc.), but in a different way. In those systems, 2D electrodes, 2D gas diffusion electrodes, or 2D membrane electrode assemblies are used adjacent to the serpentine channel, where the channel is used to distribute a gas or a liquid. Here, the main novelty lies in filling the flow channel with a 3D electrode and promoting biofilm growth. Recently, Chu and coworkers used a flow electrode-based MES reactor, which was constructed using a liquid-type flow electrode that is separated from the electrochemical cells [28]. They used powder-activated carbon as a cathode material, which was suspended in the catholyte and recirculated through the cathode compartment. The cathode compartment was a hollow serpentine channel carved into a conductive graphite sheet. This reactor differs from the concept studied here, which uses a fixed carbon felt electrode in a serpentine flow channel, with the catholyte being forced to flow through the electrode. Chu and colleagues operated their reactors in batch mode with a passive CO_2 supply from a gas bag and reported an acetate production rate of 16 ± 1 g m^{-2} day^{-1} at –5 A m^{-2}, and an acetate concentration of ~1.5 g l^{-1} both in the catholyte and extraction compartment. Other by-products were detected <0.1 g l^{-1}. Baek and coworkers designed a zero-gap MES

Glossary

Biocathode: use of microorganisms in the cathode compartment of a bioelectrochemical system, which can take up electrons (directly or indirectly) from the cathode.
Biofilm: one or several layers of microorganisms that stick to each other and often also to a solid surface (e.g., an electrode).
Current density: amount of electric current flowing per unit area (or volume) of a material (e.g., electrode, membrane, or reactor).
Faradaic efficiency: selectivity of a (bio)electrochemical process defined as the amount (moles) of collected product relative to the amount that could be produced from the total charge passed, expressed as a fraction or a percent.
Galvanostatic mode (CP): based on the control of current flowing through the system, between the working electrode and counter electrode.
Microbial electrosynthesis (MES): electricity-driven process in which microorganisms take up electrons from the cathode and reduce carbon waste, such as CO_2, to chemicals.
Ohmic drop: internal resistance that occurs due to the resistance of both the flux of electrons through the electrode materials, and the flux of ions in electrolyte solution and separator membrane.
Potentiostatic mode (CA): controls the voltage difference between a working electrode and a reference electrode, while the current flow between the working electrode and counter electrode (that completes the cell circuit) is measured.

reactor configuration with a vapor-fed anode and a liquid catholyte, which they tested for methane and acetate production from CO_2 [29]. Similarly to our design, the cathode chamber was filled with carbon felt and the catholyte was pushed through it, but a flow channel was not implemented to avoid zones with low fluid velocities. Baek and colleagues operated their reactors in batch with both bicarbonate and sporadically sparged CO_2 as a carbon source and achieved methane and acetate production rates up to 12 and 55 g m^{-2} day^{-1}, respectively, at 17.4 A m^{-2}. Quantification of biofilm growth and biomass-specific microbial rates were lacking in those studies.

The key performance indicators of the DFBR design for the production of MCCAs directly from CO_2 were investigated. We comprehensively examined the microbial growth, electrode colonization, metabolic activity, organics production, and energy efficiency over an operational period spanning 248 days. 16S rRNA-sequencing was used to identify the dominant microbial species responsible for the elongation of CO_2 to MCCAs. Our findings highlight the remarkable capability of MES to attain reactor-scale performances comparable with established technologies, establishing the viability of the novel directed-flow-through reactor as a potentially scalable system.

Results and discussion

In the current investigation, we devised an innovative MES reactor, termed a DFBR. This DFBR introduces a serpentine flow-pattern architecture in both the cathode and anode compartments. At the cathode, the serpentine channel is filled with a carbon felt electrode, through which the catholyte is forced to flow through. Two reactors were continuously operated, in either a **potentiostatic (CA) or galvanostatic (CP) mode**, for more than 220 days. Nutrients were replenished using a hydraulic retention time of 4 days, complementing the continuous sparging of CO_2.

Biomass growth rate and microbial kinetics of electrode colonization similar in potentiostatic and galvanostatic-controlled reactors

The time-dependent biomass-specific growth rate (μ) was experimentally determined for both reactors (Figure 2A), using a recently published method [30]. This method differentiates microbial growth in biofilm and in suspension. The progression of biofilm quantity per electrode volume over time and the associated percentage of electrode colonization under our experimental conditions were assessed (Figure 2B). The percentage was calculated on basis of the total biofilm amount, which reached a plateau after 225 days, representing biofilm saturation. This saturation point likely indicates a restriction in space that impeded further biofilm growth.

In both reactors, growth rates ranging from 0.03 to 0.11 day^{-1} were recorded during the initial 50 days, followed by a decline in growth rates to ~0.01 day^{-1} until the conclusion of the experiments. Comparable growth rates and trends were previously observed in nonoptimized flow-through MES reactors [30]. Consequently, the present DFBR did not speed up biofilm growth and electrode colonization. These growth rates remain modest compared with those observed in analogous anaerobic fermentation technologies, such as syngas fermentation and chain elongation (up to 2.9–5.7 day^{-1}) [31,32]. Consequently, achieving a fully grown and colonized electrode proved time-consuming in this context (225 days), underscoring the need for improvements from an application perspective. Furthermore, our observations indicated that keeping either current or potential at the used static value did not influence the growth of biofilms and electrode colonization. This suggests that electron uptake from the electrode is not the limiting process, indicating the presence of other limiting factors influencing growth. This underscores the significant challenge of rapidly colonizing a large electrode, representing a key limitation in the scale-up of MES technology.

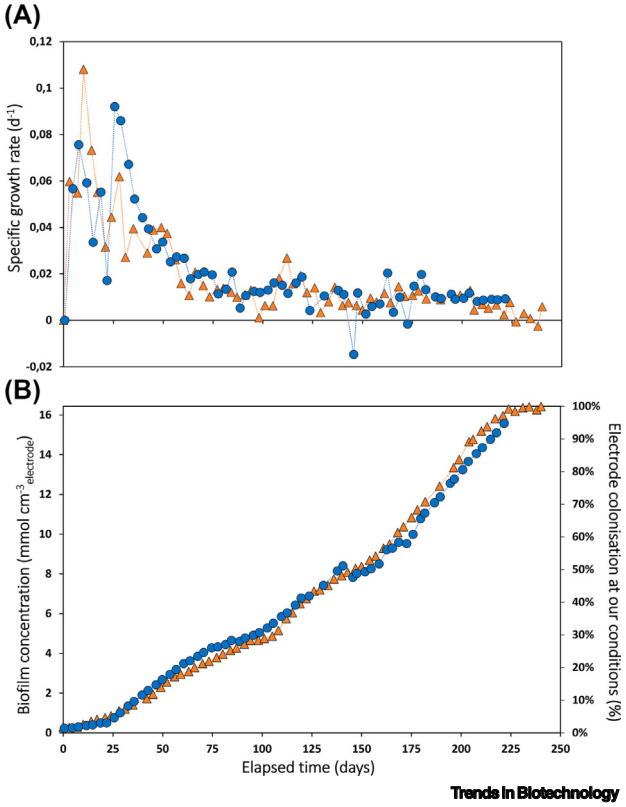

Figure 2. Microbial growth in microbial electrosynthesis reactors. (A) Biomass-specific growth rate and (B) biofilm concentration and electrode colonization measured over time in galvanostatic (CP; orange triangles) and potentiostatic (CA; blue circles) reactors.

Directed-flow-through bioelectrochemical reactor results in a three times-denser biofilm compared with previous state-of-the-art

The preceding state of the art in MES [30] achieved a biofilm apparent density, or amount of biofilm per electrode volume, of 5.0 ± 2.7 $mmol_x\ cm^{-3}_{cathode}$ (Figure S1 in the supplemental information online). By contrast, the novel serpentine design of the DFBR remarkably increased the biofilm apparent density (dry cell mass concentration) by over threefold, reaching 16.4 $mmol_x\ cm^{-3}_{cathode}$. Notably, biofilm constituted >99% of the biomass in the reactors (Figure S2 in the supplemental information online), underscoring the efficacy of the DFBR for biofilm-driven bioelectrochemical processes. Attempts to promote biofilm growth in other reactor concepts faced challenges, with microorganisms being washed out during the transition from fed-batch to continuous mode [33,34]. A higher biofilm apparent density translates into a larger number of microbes available for the target reaction. Given that inoculum and electrode material were consistent between our study and that by Winkelhorst and colleagues [30], this suggests that the reactor architecture and flow pattern/fluid dynamics had a pivotal role in the increased apparent biofilm density. The DFBR design mitigates dead zones, ensuring that the entire carbon felt is accessible for biofilm growth. Additionally, the DFBR design eliminates free-flowing liquid in the cathode chamber, facilitating transport of CO_2, nutrients, H_2, and products at the biofilm–cathode interface and throughout the channel. The catholyte superficial fluid velocity through the electrode in the DFBR was 12 times higher than reported by Winkelhorst and coworkers (20.0 vs. 1.7 mm s^{-1}), which may also have contributed to the observed biofilm density. Further

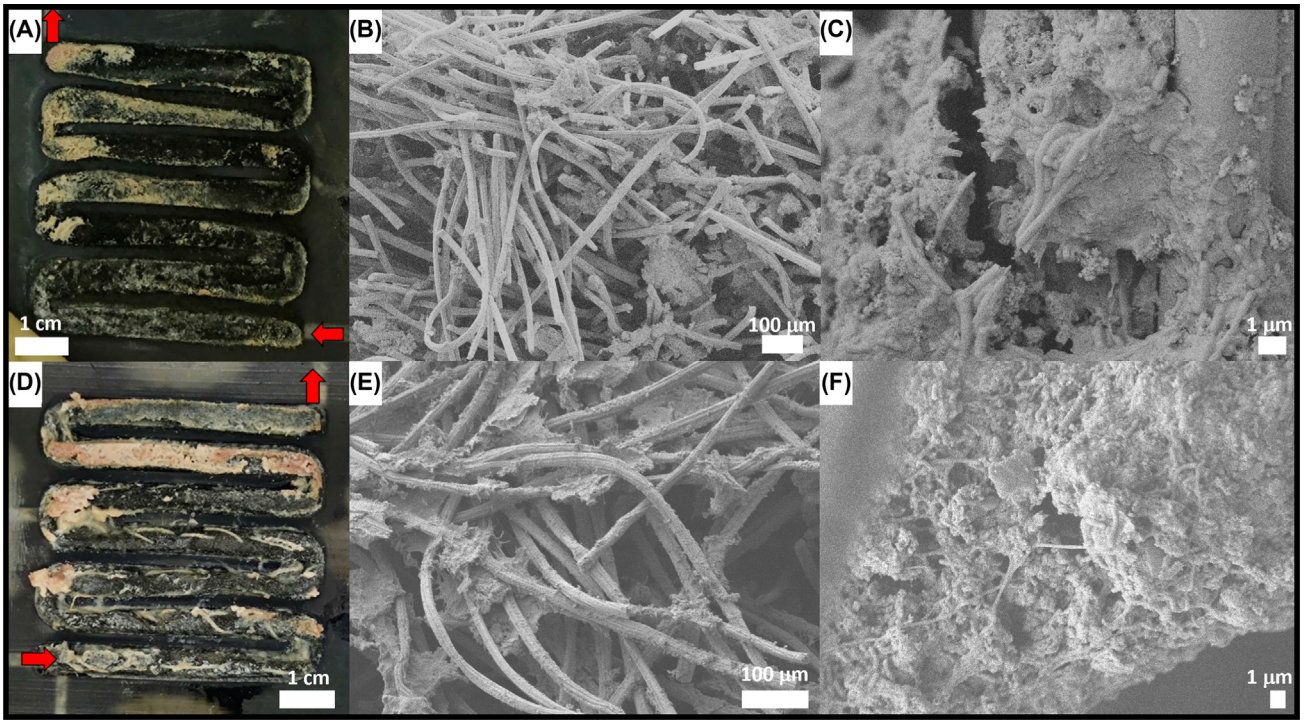

Figure 3. Photograph and scanning electron microscopy images of the biofilm grown on the carbon felt electrode of the (A–C) galvanostatic (CP) and (D–F) potentiostatic (CA) reactors at the end of the experiment. The red arrows show the inlet and outlet of the catholyte.

investigation is warranted to elucidate the impact of fluid velocity on biofilm in MES. Photographic evidence of the cathodes and scanning electron microscope (SEM) images from both reactors at the conclusion of the experiment (Figure 3 and Figure S3 in the supplemental information online) confirmed the development of a thick, dense biofilm, visible to the naked eye, on both sides of the carbon felt, spanning its entire thickness and along the entire serpentine channel. Well-formed biofilm on individual carbon fibers, comprising morphologically diverse microorganisms encapsulated in an extracellular matrix, was observable throughout the entirety of the carbon felt.

Directed-flow-through bioelectrochemical reactor results in fivefold higher volumetric current density and productivity compared with the state of the art

The evolution over time of the current density, cathode potential, organics concentration, and faradaic efficiency in both reactors were evaluated (Figure 4). The trends in organics production rates and current normalized to electrode volume are depicted in Figures S4 and S5 in the supplemental information online. Notably, no alcohols, such as ethanol, were detected at any point during the experiments.

In the CP reactor, the cathode potential consistently ranged between –0.8 V and –1.0 V versus a standard hydrogen electrode (SHE) throughout successive applied current steps, reaching up to –105 A m^{-2}_{PSA} (projected surface area). In the CA reactor (-0.85 V vs. SHE), the cathodic current initially remained low at around –5 A m^{-2}_{PSA} for the first 25 days, gradually increasing to –15 A m^{-2}_{PSA} by Day 35. Subsequently, the current remained relatively stable until Day 85, coinciding with ~30% biofilm colonization of the carbon felt (Figure 2B). Between Day 85 and Day 139, the current exhibited exponential growth, reaching –100 A m^{-2}_{PSA}, corresponding to 50% biofilm

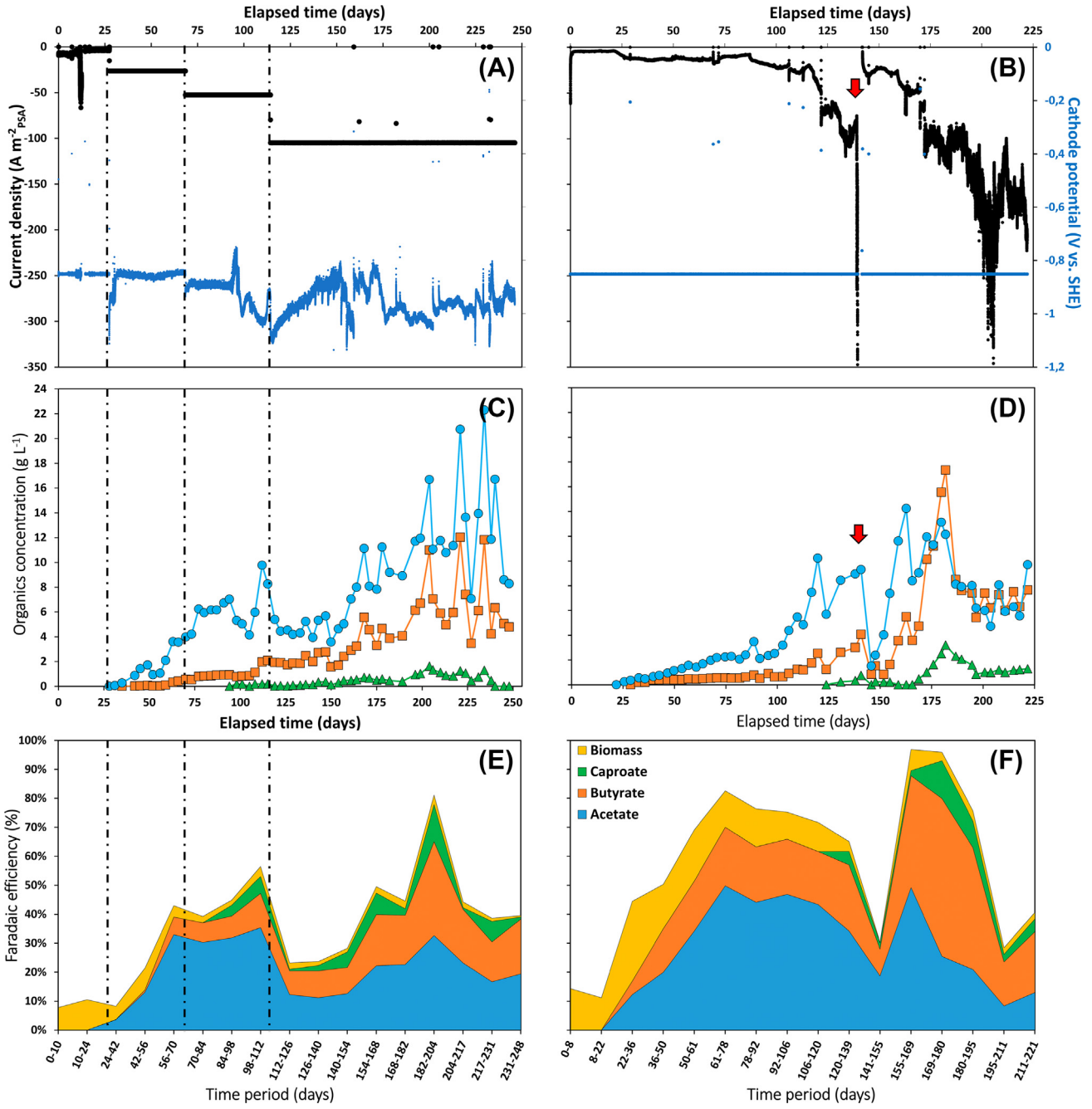

Figure 4. Key performance indicators at reactor's scale. (A,B) Current density and cathode potential, (C,D) concentration of acetate (blue circles), butyrate (orange squares), and caproate (green triangles), and (E,F) faradaic efficiency evolution over time in the galvanostatic (CP; left) and potentiostatic (CA; right) reactors. The red arrow (Day 139) indicates a leakage event that emptied the cathode compartment almost entirely, which stopped the potentiostat and liquid recirculation; the reactor remained in this state for 3 days (long weekend).

coverage on the carbon felt. The reactor experienced a crash on Day 139, inducing biofilm stress, resuspension, and rapid reattachment, evident by a sudden increase and subsequent decrease in optical density (Figure S6 in the supplemental information online). Following a lag phase, the

electron uptake rate recovered from Day 170 and remarkably surged further to a cathodic current of approximately –200 A m^{-2}_{PSA} (–40 mA $cm^{-3}_{cathode}$) at the conclusion of the experiment, with peaks reaching –300 A m^{-2}_{PSA} (–60 mA $cm^{-3}_{cathode}$) over a 7-day period between Days 200 and 207. The prior state-of-the-art MES reactor, producing soluble organics, reported a current of –101 A m^{-2}_{PSA}, equivalent to –7.8 mA $cm^{-3}_{cathode}$, at the same cathode potential [6]. The DFBR demonstrated a notable enhancement, achieving a twofold increase in current normalized to projected surface area and a fivefold increase in volume of the electrode. Normalizing performance to electrode volume is particularly relevant when using 3D electrodes [35,36], accounting for the electrode thickness. The previous state-of-the-art current of –101 A m^{-2}_{PSA} was attained with a 1.2 cm-thick carbon felt, whereas we used a 0.5 cm-thick carbon felt. A thinner cathode is advantageous, promoting lower ohmic resistances and, consequently, higher energy efficiencies [2,11]. In the final 10 days of the experiment, a faradaic efficiency of 40% (and increasing) was achieved, corresponding to VPs of 43 kg_{C2} $m^{-3}_{cathode}$ day^{-1}, 30 kg_{C4} $m^{-3}_{cathode}$ day^{-1}, and 5 kg_{C6} $m^{-3}_{cathode}$ day^{-1} (equivalent to a total carbon production of 37.3 kg_C $m^{-3}_{cathode}$ day^{-1}).

Biofilm suspension and reattachment lead to higher carbon selectivity and faradaic efficiency into C4 and C6

Within the initial 25 days, only biomass growth occurred, representing ~11.3 ± 2.9% of electron recovery into biomass in both reactors, at comparable current densities. Consequently, both reactors exhibited a lag phase of ~25 days before measurable amounts of soluble organics were produced, a phenomenon previously observed in MES [30,37]. Acetate (C2) was the initial product in both reactors, closely followed by n-butyrate (C4). During the initial 100 days, under CP, C2 and C4 concentrations increased more rapidly than under CA (7.0 versus 2.5 g_{C2} l^{-1} and 0.9 vs. 0.6 g_{C4} l^{-1}), albeit at the expense of faradaic efficiency (45% vs. 75%), likely due to higher currents (i.e., higher availability of H_2). A lower faradaic efficiency corresponds to reduced energy efficiency (Figure S7 in the supplemental information online), indicating higher energy wastage. Application of a higher current (CP) than that measured under CA did not result in increased growth rates or higher biofilm amounts (28% electrode colonization in both reactors at Day 100; Figure 2). However, it did lead to higher acetate production rates in the first 100 days (26 vs. 10 kg_{C2} $m^{-3}_{cathode}$ day^{-1}; Figure S4), likely due to a higher H_2 availability, suggesting a decoupling of growth and production metabolisms. As observed previously, once a mature biofilm was established, carboxylate production became maintenance driven [30]. This pattern persisted here, with acetate concentration reaching up to 10 g l^{-1} and productivity 34 kg_{C2} $m^{-3}_{cathode}$ day^{-1} when the current density increased to similar, and subsequently higher, levels under CA from Day 125 to 139 (up to –100 A m^{-2}). Simultaneously, the butyrate concentration reached 4 g l^{-1} and productivity 18 kg_{C4} $m^{-3}_{cathode}$ day^{-1}. A higher faradaic efficiency of 65% was achieved at –100 A m^{-2} under CA compared with –52 A m^{-2} under CP (50%). Caproate (C6) production started earlier under CP than CA (98 vs. 130 days), likely attributable to the earlier attainment of higher concentrations of C2 and C4 [6,18].

Following the lag phase subsequent to the CA reactor crash on Day 139, a notable faradaic efficiency of 90% was achieved from Day 155 to 169 at a current density of approximately –47 A m^{-2}. An even higher faradaic efficiency of 93% was reached at –102 A m^{-2}_{PSA} (–20 mA $cm^{-3}_{cathode}$) from Day 169 to 180, coinciding with elevated concomitant VPs of 50 kg_{C2} $m^{-3}_{cathode}$ day^{-1}, 71 kg_{C4} $m^{-3}_{cathode}$ day^{-1}, and 15 kg_{C6} $m^{-3}_{cathode}$ day^{-1} (equivalent to 69 kg_C $m^{-3}_{cathode}$ day^{-1}). This represents a remarkable 3.1-fold increase in soluble organics productivity compared with the state of the art (22 kg_C $m^{-3}_{cathode}$ day^{-1}) [6]. Notably, a high carbon selectivity of 57%$_{C4}$ and 14%$_{C6}$ (Figure S8 in the supplemental information online) and a faradaic efficiency of 55%$_{C4}$ and 13%$_{C6}$ into C4 and C6, respectively, were achieved. Higher selectivity toward C4 and C6 is advantageous given their higher value compared with acetate [4]. Lower carbon selectivity

(29%$_{C4}$ and 4%$_{C6}$) and faradaic efficiency (23%$_{C4}$ and 5%$_{C6}$) into C4 and C6 were recorded before the reactor crash at the same current density of –102 A m^{-2}_{PSA} from Day 120 to 139. Similarly, a lower carbon selectivity (36 ± 6%$_{C4}$ and 8 ± 5%$_{C6}$) and faradaic efficiency (16 ± 7%$_{C4}$ and 4 ± 4%$_{C6}$) into C4 and C6 were achieved in the CP reactor at –105 A m^{-2}, which did not experience significant biofilm disturbance. A previous study also demonstrated that rapid detachment and reattachment, leading to biofilm reorganization, significantly improved carbon selectivity and faradaic efficiency toward C4 and C6 over acetate [18]. The mechanism responsible for this phenomenon is yet to be fully elucidated. A lower total faradaic efficiency was recorded from Day 120 to 139 (62%) compared with Day 169 to 180 (93%) at the same current density in the CA reactor. This discrepancy may be attributed to a lower biofilm amount (7.4 vs. 10.8 $mmol_x$ $cm^{-3}_{cathode}$) and electrode coverage (43 versus 68%) (Figure 2B) and/or to the biofilm reorganization.

The faradaic efficiency declined notably after the escalation of current density to –200 A m^{-2}_{PSA} (–40 mA $cm^{-3}_{cathode}$) from Day 195 to 221. The cause of this surge in cathodic current remains unclear, but it might be attributed to the increase in electrode coverage by biofilm to over 90% during that period (Figure 2B). A higher biofilm amount correlates with an increased demand for electrons. On Day 180, the highest concentrations ever reported in continuously operated MES reactors of C4 (17.4 g l^{-1}) and C6 (3.2 g l^{-1}) were reached. Subsequently, a decline in organics concentration and production rates was observed. A plausible explanation could be inhibition of the biofilm by C4 and C6 acids, known for their toxicity, as previously modeled in MES [13], although further investigation is required for confirmation. Nonetheless, a twofold higher VP compared with the previous state of the art was maintained from Day 195 until the conclusion of the experiment. Additionally, carbon selectivity remained favorable, with 57% and 11% directed into C4 and C6, respectively.

When comparing our results with those of Chu and Baek and colleagues, who studied a flow-electrode-based MES reactor and a zero-gap MES reactor, respectively, an order of magnitude higher current density, productivity, and product concentration were obtained with our DFBR, while producing significant amounts of butyrate and caproate in addition to acetate (and no methane). Combining a vapor-fed anode as tested by Baek and coworkers with our cathode configuration could be a promising avenue to further increase the energy efficiency of MES while achieving high productivity.

Potentiostatic control results in higher faradaic and energy efficiencies under our conditions

Under galvanostatic control (CP), an increment in cathodic current density from –26 to –53 or –105 A m^{-2} did not significantly elevate the organics concentration until Day 150 (Figure 4C). This observation could be attributed to the fact that, by Day 150, only half of the electrode was colonized (Figure 2B). The limited biofilm coverage hampers the microbial uptake of electrons (and CO_2). This is evident in the relatively low faradaic efficiency during this period. Subsequently, from Day 150 until the end of the experiment, concentrations and production rates gradually increased as biofilm coverage expanded. High acetate and butyrate concentrations of 22.3 g l^{-1} and 12 g l^{-1} were attained in this reactor. Simultaneous VPs of 64 kg_{C2} $m^{-3}_{cathode}$ day^{-1}, 42 kg_{C4} $m^{-3}_{cathode}$ day^{-1}, and 17 kg_{C6} $m^{-3}_{cathode}$ day^{-1} (equivalent to 60 kg_C $m^{-3}_{cathode}$ day^{-1}) were achieved (Figure S4), marking a 2.7-fold increase compared with the previous state of the art and similar to the CA reactor. Relative to the CA reactor, lower faradaic and energy efficiencies were observed under galvanostatic control, despite similar current density and biofilm amount/coverage. The reasons for these differences warrant further investigation. In the CA reactor, energy efficiencies averaged 34 ± 17% at –102 A m^{-2}, with a peak at 64% (Figure S7). However, optimizing the energy efficiency of the DFBR was beyond the scope of this work; for instance, a thick membrane was used, leading to high ohmic overpotentials. Overall, CP did not accelerate biofilm growth or result in higher organics productivity and faradaic efficiency in this study.

Biomass-specific production rates maintained over a long period of time

Using a recently established methodology [30], biomass-specific production rates (q_p) can now be determined over time in MES (Figure 5). Biomass-specific production rate represents a microbial kinetic parameter that normalizes the production rate to the quantity of biomass within the reactor at a specific moment. Utilizing biomass-specific rates, one can more effectively assess the specific performance of the biocatalysts in MES, facilitating meaningful comparisons with other technologies.

In both reactors, q_p exhibited an initial increase before stabilizing at comparable values of 0.19 ± 0.06 mol_C mol_x^{-1} day^{-1} until the conclusion of the experiments. A preceding study, which reported q_p in MES, documented biomass-specific production rates of C2–C6 carboxylates of ~0.25 ± 0.05 mol_C mol_x^{-1} day^{-1} over the initial 50 days, followed by a gradual decline to 0.05 ± 0.03= mol_C mol_x^{-1} day^{-1} by Day 200 [30]. It was suggested that this rate, similar to the specific growth rate, declined as the biofilm quantity increased and matured to fully colonize the electrode. The aforementioned study utilized nonoptimized flow-through reactors with the same electrode material and inoculum. By contrast, our findings demonstrate that the novel DFBR concept allows for the preservation of biomass-specific production rates over an extended period, even with biofilm apparent density three times higher and elevated product concentrations compared with the study by Winkelhorst and colleagues [30]. These results can be attributed to improved mass transport of CO_2, nutrients, H_2, and/or products throughout the entire cathode, facilitated by the specific reactor architecture and fluid dynamics.

Volumetric productivity in MES now comparable with syngas fermentation

Syngas fermentation serves as a pertinent benchmark for assessing MES. Syngas fermentation, using acetogens to convert gas mixtures of H_2, CO, and CO_2 into a mixture of acetate and ethanol, has been successfully scaled up to an industrial level, exemplified by the LanzaTech process [7]. When comparing these technologies, three technical key performance indicators [biomass-specific production rates (q_p), the amount of biomass per reactor volume, and the product of

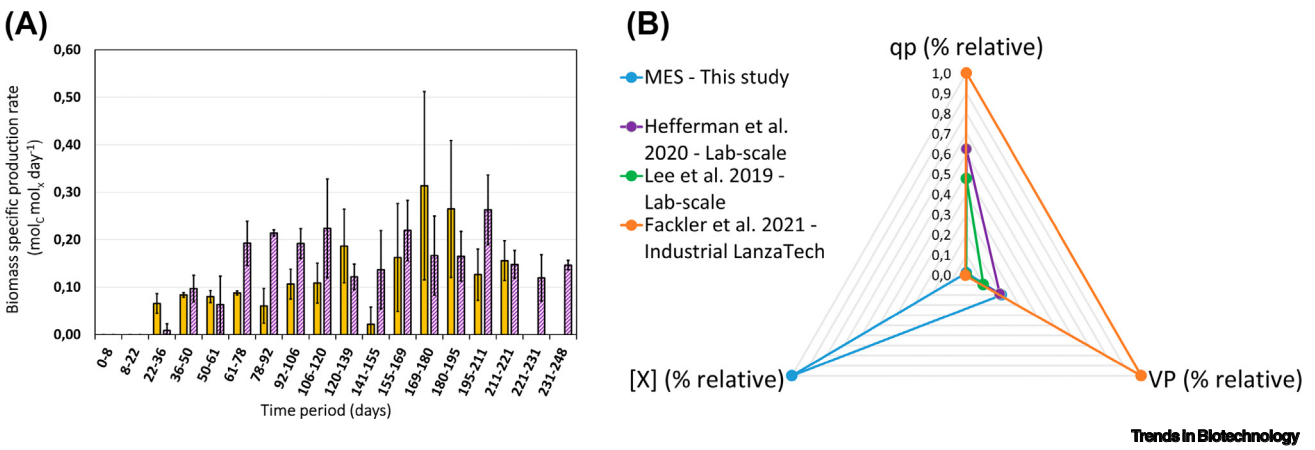

Figure 5. Microbial electrosynthesis from CO_2 versus syngas fermentation. (A) Biomass-specific production rates measured over time in the galvanostatic (CP; purple bars) and potentiostatic (CA; yellow bars) reactors. (B) Comparison of three key performance indicators between our microbial electrosynthesis (MES) reactor and two of the best-performing laboratory-scale syngas fermentation reported in the literature [8,9], as well as the industrial LanzaTech7 syngas fermentation process [7]. Instead of absolute values for each key performance indicator (KPI), the relative percentages calculated from the maximum value are represented. Biomass-specific production rates (q_p) vary from 0.2 to 20 mol_C mol_x^{-1} day^{-1}, biomass concentrations [X] from 0.5 to 390 g_x l^{-1}, and volumetric productivities (VPs) from 0.1 to 1 g_C l^{-1} h^{-1}. Here, VP is normalized to the total medium volume, and not to the cathode volume in MES. Table S1 in the supplemental information online details the values extracted from the literature and used here. See [7–9]. Table S2 in the supplemental information online shows the KPIs of other syngas fermentation studies.

both, i.e., the VP] should be considered. A comparison was drawn using data from two laboratory-scale syngas fermentation studies reporting the highest performance to the best of our knowledge [8,9], and the industrial-scale LanzaTech process (Figure 5B) [7]. The achieved biomass-specific production rates in MES were notably lower than those reported in syngas fermentation, reaching up to 20 $mol_C\ mol_x^{-1}\ day^{-1}$. This observation presents an opportunity for MES, indicating the potential for higher microbial rates. Conversely, the amount of microbial biomass per unit of reactor volume in MES (390 $g_x\ l^{-1}{}_{cathode}$) significantly surpassed that in syngas fermentation (2.5 $g_x\ l^{-1}$). MES relies on a dense biofilm, while the highest syngas fermentation performances were attained with microorganisms in suspension. Consequently, our MES process demonstrated a comparable VP of ~0.2 $g_C\ l^{-1}\ h^{-1}$ to laboratory-scale syngas fermentation and was five times lower than achieved with the LanzaTech process. The VP calculations in MES here utilized the total volume of catholyte, including the catholyte in the tubing and in the bubble column. Comparing volumetric production rates between biofilm-based and planktonic-based systems makes sense because the product is soluble in the medium. Normalizing to the volume of catholyte in the cathode chamber yielded productivity values 14 times higher, surpassing the LanzaTech process by 2.5 times. Optimization of the catholyte to electrode volume ratio requires further investigation. Additionally, considering market prices, it is noteworthy that C4 and C6 carboxylic acids, produced in MES, have higher prices than ethanol, although their market volumes are lower [4]. Actual scale-up of MES and in-depth techno-economic assessment of both technologies must then be performed to compare them fairly. Both technologies may also be complementary. This study represents a milestone in developing MES as a competitive technology, marking a promising outcome that warrants further scaling up of MES technology.

Furthermore, microbial rates in MES are within the same order of magnitude as rates achieved in gas fermentation converting H_2 + CO_2 to carboxylates [8,38,39]. In a study by Zhang and colleagues [38], biofilms were cultivated on hollow-fiber membranes to convert an H_2/CO_2 mixture, yielding volumetric production rates considerably lower at 0.003 $g_C\ l^{-1}\ h^{-1}$ compared with the rates reported in our study. Another study by Kantzow and coworkers reported the use of a standard stirred-tank bioreactor equipped with a customized submerged microfiltration unit for biomass retention [40]. Continuously supplying CO_2–H_2 gas mixture and yeast extract resulted in 14 g l^{-1} of cell dry weight and 2.5 $g_C\ l^{-1}\ h^{-1}$ of acetate. A systematic comparison of these two technologies is essential to delineate the advantages and disadvantages of each approach, especially in the context of scale-up considerations. Notably, Roghair and colleagues reported higher biomass-specific rates of 10 $mol_C\ mol_x^{-1}\ day^{-1}$ in their fermentation process, converting acetate and ethanol to a mixture of C2–C6 carboxylates, accompanied by a VP of 2.7 $g_C\ l^{-1}\ h^{-1}$ [41]. Such comparative analyses can contribute valuable insights into optimizing and advancing these microbial processes.

The calculated biomass-specific production rates (q_p) in MES presented in this study are underestimated, because they do not consider the accumulation of dead biomass within the biofilm. Winkelhorst and coworkers demonstrated that, after 200 days, up to 50% of the microbes within the biofilms were dead [30]. Consequently, the estimated q_p values were approximately half of the actual values, emphasizing the need to account for dead biomass to obtain a more accurate assessment of microbial kinetics in MES. Moreover, the maximum theoretical amount of dry biomass per electrode volume should not exceed 12 mmol cm^{-3}, (based on a cell density of 1.09 g cm^{-3}, a dry weight ratio of 30%, and a carbon felt porosity of 90%; see calculations in the supplementary information online). However, we calculated a maximum of 16.4 $mmol_x\ cm^{-3}{}_{cathode}$, which is 37% higher than the theoretical maximum. This may be due to approximations in the N-balance method used for biomass quantification [30]. Therefore, the estimated μ and q_p values may be at least 37% higher than reported earlier. Nevertheless, the VPs remain

true and comparable with VP achieved in syngas fermentation. Even if the actual biomass-specific production rates were two to three times higher than reported above (i.e., up to 0.6 $mol_C\ mol_x^{-1}\ day^{-1}$), this would still be more than 30 times lower than microbial kinetics reported in syngas fermentation (20 $mol_C\ mol_x^{-1}\ day^{-1}$), which means that microbial kinetics in MES can be improved further.

Clostridium luticellarii and *Eubacterium limosum* are dominant species

To gain a deeper understanding of the notable performance distinctions between potentiostatically (CA) operated bioreactors and their galvanostatically (CP) controlled counterparts, we used high-throughput 16S rRNA gene sequencing to investigate microbial community structures. Following an experimental period exceeding 220 days, microbial samples were collected from cathode-attached cells at three locations along the serpentine flow channel (Figure 6A). Each sample exhibited a dominant amplicon sequence variant (ASV) representation of more than 65%, encompassing no more than seven ASVs. Across the six samples, only 13 dominant species were identified (Figure 6B). Four species (*Eubacterium limosum*, *Eubacterium callanderi, Fermentimonas caenicola,* and *Clostridium luticellari*) were consistently present in all samples, regardless of the operational mode.

Among the remaining nine species, eight were specific to a single process. The CP reactor consistently featured ASVs belonging to the *Methanobrevibacter* and *Pseudoclavibacter* genera. By contrast, microbial communities from the CA reactor consistently shared six species, including *Oscillibacter* and *Phocaeicola* ASVs, in addition to the four species systematically found. Strikingly, none of these 13 ASVs have been previously associated with MES microbial communities [42–44].

Three of the four systematically identified dominant species (*E. limosum*, *E. callanderi*, and *C. luticellari*) belong to the Clostridia class. These are known acetogens typically found in microbial communities associated with syngas fermentation. In this process, they grow autotrophically by utilizing a mixture of H_2, CO, and CO_2 as carbon and energy sources, converting them into the central intermediate acetyl-CoA, which is converted to acetate by most acetogens [45].

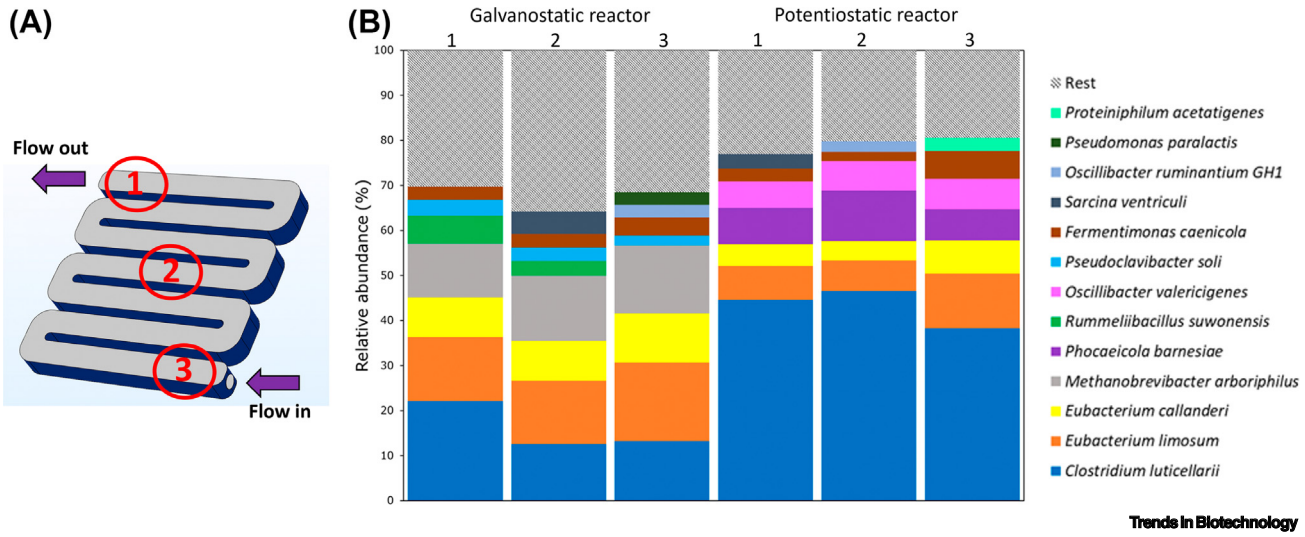

Figure 6. Microbial community analysis. (A) Sampling location along the serpentine electrode. (B) Relative abundance of 16S rRNA of bacterial samples taken from three locations in both the galvanostatic (CP) and potentiostatic (CA) reactors at the end of the experiment.

Interestingly, *E. limosum* and *C. luticellari* were also found to perform chain elongation and produce C4 and C6 carboxylic acids [45,46], a characteristic dependent on environmental conditions. Reasons for the presence of the three anaerobic species (*Phocaeicola barnesiae* [47], *Oscillibacter valericigenes*, and *Fermentimonas caenicola*) remain unclear. Only *O. valericigenes* (*Clostridia* class) was linked to C5 carboxylic acid biosynthesis [48]. The presence of these ancillary species could be necessary to meet specific nutritional requirements and contribute to the stable establishment of the biofilm.

On basis of these initial taxonomic findings, it is inferred that the serpentine design, which establishes a flow pattern in the forced-flow-through reactor, enabling an extended residence time for nutrients, CO_2, H_2, and products within the 3D-electrode, did not yield a pronounced gradient in community composition along the flow channel in each reactor. The microbial composition was found to be comparable at all three locations. It is essential to underscore that relative abundance does not necessarily align with activity levels. To understand the microbial function and physiology of these highly active biofilms, further analyses involving metagenomics, metatranscriptomics, and metaproteomics are imperative.

The source of the biofilm inoculum has a pivotal role in shaping the composition of the ultimate microbial community, and the considerable diversity in inoculum origins documented in scientific literature poses challenges for meaningful comparisons. Nonetheless, our results conclusively demonstrate that novel microbial communities capable of driving highly efficient processes can be assembled in MES bioreactors.

Concluding remarks

We established that forcing an electron flow through the application of current does not accelerate the growth of biofilms. This investigation underscores that the primary constraint to the applicability of MES lies in the rate at which a large electrode can be colonized (see Outstanding questions). Mass transport of nutrients, CO_2, and products, fluid dynamics through the electrode, and medium compositions could help alleviate growth limitations. Once colonization occurred, we demonstrated a threefold higher volumetric current density and productivity compared with the state of the art, up to a new record of –28 ± 7 mA $cm^{-3}_{cathode}$ (–142 ± 39 A m^{-2}) and 43 ± 24 kg_C $m^{-3}_{cathode}$ day^{-1}, sustained over 50 days. Maximum production of 69 kg_C $m^{-3}_{cathode}$ day^{-1} was recorded over periods of more than 15 days. Faradaic and energy efficiencies of 60–97% and 30–35% were achieved, respectively. The designed DFBR showcased in this work enables the achievement of elevated biofilm concentrations per electrode volume, sustained microbial activity over a period exceeding 225 days, and notable volumetric productivity, now comparable with rates observed in syngas fermentation.

This study emphasizes the feasibility of enhancing microbe-specific rates to further increase volumetric productivity and product selectivity. Uncovering the exact electron transfer mechanisms from CO_2 to C6 will help gain control over the process. A compromise must be found between having enough electrode surface area for sufficient biofilm coverage (i.e., for high organics production rates) and efficient mass transport and fluid dynamics through the 3D/filamentous electrode. Another aspect to improve is the stability of production. Where syngas fermentations are generally stable in terms of production rates, MES currently shows instability over time. Moreover, high CO_2 conversion efficiencies should be aimed at when scaling up to larger reactor sizes, which could be promoted with long flow channels, as proposed here. Another aspect to optimize is the catholyte:electrode volume ratio, which can be tuned to increase volumetric productivity, while avoiding product inhibition and allowing sufficient mass transport. In addition, the volume of the anolyte and/or the design of the anode compartment should be considered and optimized upon scale-up. VP rate accounting for the whole

Outstanding questions

How can microbial growth rate be increased to fully colonize an electrode more quickly? How can microbe-specific production rates be further enhanced?

What are the electron transfer mechanisms from the electrode to hexanoic acid?

Can production stability be achieved and/or can control be gained over microbial and reactor performance?

Can this directed flow-through MES reactor concept be physically scaled up to relevant size in a techno-economic way (including energy consumption)?

Should open microbial cultures, synthetic mixed cultures, or pure cultures be used for industrial applications?

reactor volume must be considered when comparing with other technologies. Here, we disregarded the anolyte volume because optimizing the anode compartment was out of the scope of this study. Given that the anode compartment was identical to the cathode compartment, one can apply a factor of two to calculate the reactor-scale VP rate from the reported values.

A practical challenge to the proposed design approach is the energy needed to force the catholyte through the carbon felt. Here, an overpressure of 0.4–0.7 bar was measured over a 40 cm-long flow channel at the end of the experiments (Figure S6). The overpressure increased over time as the biofilm grew, which led to more fluid channels within the carbon felt to clog (Figures 3 and S3). Upon scale-up, a high overpressure would require more pumping energy, ultimately decreasing the overall energy efficiency. Further research should look at ways to minimize the pressure drop, such as using electrodes with a more open structure.

Inhibiting methanogenesis in a cost-effective way when using a mixed microbial culture remains a pressing challenge. Continuously feeding an expensive compound, such as sodium-bromoethanesulfonate, is not a solution.

Society needs sustainable carbon-based chemicals and several feedstock and technologies will be needed to satisfy the demand. CO_2 is an attractive feedstock, because it is widely available and must be taken out of the atmosphere. Beyond laboratory-scale research, MES has the potential to be one of those technologies that transform the chemical industry and provide sustainable products to the society. MES distinguishes itself from other CO_2-conversion technologies, such as CO_2 electrolysis (using heterogeneous catalysts) or plasma technology, as it can produce more complex molecules, with more than two carbons. Therefore, MES does not compete with these technologies, as different markets and applications are targeted. MES also does not heavily rely on metals for which availability and supply chain challenges may arise in the future, and instead uses cheap carbon electrodes and microorganisms. Another advantage is that microbial biofilms in MES are self-repairing and robust, which has been demonstrated with reactors operated for more than 2 years. Thus, the results presented here represent a milestone in developing MES as a competitive technology for efficient CO_2 valorization.

STAR★METHODS

Detailed methods are provided in the online version of this paper and include the following:

- KEY RESOURCES TABLE
- METHOD DETAILS
  - MES reactor setup
  - MES reactor operation
  - Analytical methods
  - Scanning electron microscopy
  - DNA extraction and 16S sequence analysis
  - Microbial community analysis

RESOURCE AVAILABILITY

Lead contact

Further information and requests for resources should be directed to and will be fulfilled by the Lead Contact, Ludovic Jourdin (l.jourdin@tudelft.nl).

Materials availability

This study did not generate new unique materials.

Data and code availability

The data underlying the publication are publicly available on 4TU.ResearchData, DOI 10.4121/28d4cf06-85e2-4c63-a632-179ede79251f, in line with the TU Delft Research Data Framework Policy. Metagenomic V3-V4 16S rRNA gene Amplicon DNA-sequencing data of cathode microbiome were deposited at NCBI (https://www.ncbi.nlm.nih.gov/) under BioProject accession number PRJNA1071877.

Author contributions

O.C.P., M.W., and R.K.A. operated the MES reactors. O.C.P. and L.J. designed the study and the novel reactor, analyzed and interpreted the data, and drafted the manuscript. R.S. and J.M.D. analyzed the microbial communities and drafted the manuscript. K.M. 3D-printed the reactors. L.J., J.M.D., and A.J.J.S. acquired the funding. All authors contributed to manuscript revision, conception, and read and approved the submitted version.

Acknowledgments

This activity was co-financed by Shell and a PPP-allowance from Top Consortia for Knowledge and Innovation (TKIs) of the Dutch Ministry of Economic Affairs and Climate in the context of the TU Delft e-Refinery Institute. R.S., J.M.D., and L.J. acknowledge the co-financing by DSM-Firmenich and a PPP-allowance from Top Consortia for Knowledge and Innovation (TKIs) of the Dutch Ministry of Economic Affairs and Climate. The authors thank Scixel for designing the graphical abstract.

Declaration of interests

L.J. and O.C.P. have a patent pending related to this work (NL2032221).

Supplemental information

Supplemental information to this article can be found online at https://doi.org/10.1016/j.tibtech.2024.06.005.

References

1. Rabaey, K. and Rozendal, R.A. (2010) Microbial electrosynthesis — revisiting the electrical route for microbial production. *Nat. Rev. Micro* 8, 706–716
2. Jourdin, L. and Burdyny, T. (2020) Microbial electrosynthesis: where do we go from here? *Trends Biotechnol.* 39, 359–369
3. Flexer, V. and Jourdin, L. (2020) Purposely designed hierarchical porous electrodes for high rate microbial electrosynthesis of acetate from carbon dioxide. *Acc. Chem. Res.* 53, 311–321
4. Jourdin, L. *et al.* (2020) Techno-economic assessment of microbial electrosynthesis from CO2 and/or organics: an interdisciplinary roadmap towards future research and application. *Appl. Energy* 279, 115775
5. Vassilev, I. *et al.* (2018) Microbial electrosynthesis of isobutyric, butyric, caproic acids, and corresponding alcohols from carbon dioxide. *ACS Sustain. Chem. Eng.* 6, 8485–8493
6. Jourdin, L. *et al.* (2018) Critical biofilm growth throughout unmodified carbon felts allows continuous bioelectrochemical chain elongation from CO2 up to caproate at high current density. *Front. Energy Res.* 6, 7
7. Fackler, N. *et al.* (2021) Stepping on the gas to a circular economy: accelerating development of carbon-negative chemical production from gas fermentation. *Annu. Rev. Chem. Biomol. Eng.* 12, 439–470
8. Heffernan, J.K. *et al.* (2020) Enhancing CO2-valorization using *Clostridium autoethanogenum* for sustainable fuel and chemicals production. *Front. Bioeng. Biotechnol.* 8, 204
9. Lee, J. *et al.* (2019) Domestication of the novel alcohologenic acetogen *Clostridium* sp. AWRP: from isolation to characterization for syngas fermentation. *Biotechnol. Biofuels* 12, 228
10. Nevin, K.P. *et al.* (2010) Microbial electrosynthesis: feeding microbes electricity to convert carbon dioxide and water to multicarbon extracellular organic compounds. *mBio* 1, e00103-10
11. Prévoteau, A. *et al.* (2020) Microbial electrosynthesis from CO2: forever a promise? *Curr. Opin. Biotechnol.* 62, 48–57
12. Vassilev, I. *et al.* (2022) Cathodic biofilms – a prerequisite for microbial electrosynthesis. *Bioresour. Technol.* 348, 126788
13. Cabau-Peinado, O. *et al.* (2021) A general model for biofilm-driven microbial electrosynthesis of carboxylates from CO2. *Front. Microbiol.* 12, 669218
14. Kühl, M. and Jørgensen Bo, B. (1992) Microsensor measurements of sulfate reduction and sulfide oxidation in compact microbial communities of aerobic biofilms. *Appl. Environ. Microbiol.* 58, 1164–1174
15. Picioreanu, C. *et al.* (2007) A computational model for biofilm-based microbial fuel cells. *Water Res.* 41, 2921–2940
16. Picioreanu, C. *et al.* (2000) A theoretical study on the effect of surface roughness on mass transport and transformation in biofilms. *Biotechnol. Bioeng.* 68, 355–369
17. Alqahtani, M.F. *et al.* (2018) Porous hollow fiber nickel electrodes for effective supply and reduction of carbon dioxide to methane through microbial electrosynthesis. *Adv. Funct. Mater.* 28, 1804860
18. Jourdin, L. *et al.* (2019) Enhanced selectivity to butyrate and caproate above acetate in continuous bioelectrochemical chain elongation from CO2: steering with CO2 loading rate and hydraulic retention time. *Bioresour. Technol. Rep.* 7, 100284
19. Krieg, T. *et al.* (2019) Reactors for microbial electrobiotechnology. *Adv. Biochem. Eng. Biotechnol.* 167, 231–271
20. Cui, K. *et al.* (2023) An electrolytic bubble column with an external hollow fiber membrane gas–liquid contactor for effective microbial electrosynthesis of acetate from CO2. *Chem. Eng. J.* 471, 144296
21. Rosa, L.F.M. *et al.* (2017) Paving the way for bioelectrotechnology: integrating electrochemistry into bioreactors. *Eng. Life Sci.* 17, 77–85
22. Rosa, L.F.M. *et al.* (2019) Integrating electrochemistry into bioreactors: effect of the upgrade kit on mass transfer, mixing time and sterilizability. *Front. Energy Res.* 7, 98
23. Enzmann, F. *et al.* (2019) Transferring bioelectrochemical processes from H-cells to a scalable bubble column reactor. *Chem. Eng. Sci.* 193, 133–143

24. Batlle-Vilanova, P. *et al.* (2017) Microbial electrosynthesis of butyrate from carbon dioxide: Production and extraction. *Bioelectrochemistry* 117, 57–64
25. Romans-Casas, M. *et al.* (2021) Bio-electro CO2 recycling platform based on two separated steps. *J. Environ. Chem. Eng.* 9, 105909
26. Roy, M. *et al.* (2023) Scalability of the microbial electroacetogenesis process for biogas upgradation: performance and technoeconomic assessment of a liter-scale system. *Energy Fuel* 37, 15822–15831
27. de Smit, S.M. *et al.* (2023) Alternating direction of catholyte forced flow-through 3D-electrodes improves start-up time in microbial electrosynthesis at applied high current density. *Chem. Eng. J.* 464, 142599
28. Chu, N. *et al.* (2023) Flow-electrode microbial electrosynthesis for increasing production rates and lowering energy consumption. *Engineering* 25, 157–167
29. Baek, G. *et al.* (2022) High-rate microbial electrosynthesis using a zero-gap flow cell and vapor-fed anode design. *Water Res.* 219, 118597
30. Winkelhorst, M. *et al.* (2023) Biomass-specific rates as key performance indicators: a nitrogen balancing method for biofilm-based electrochemical conversion. *Front. Bioeng. Biotechnol.* 11, 1096086
31. Groher, A. and Weuster-Botz, D. (2016) General medium for the autotrophic cultivation of acetogens. *Bioprocess Biosyst. Eng.* 39, 1645–1650
32. Candry, P. *et al.* (2018) A novel high-throughput method for kinetic characterisation of anaerobic bioproduction strains, applied to *Clostridium kluyveri*. *Sci. Rep.* 8, 9724
33. Arends, J.B.A. *et al.* (2017) Continuous long-term electricity-driven bioproduction of carboxylates and isopropanol from CO2 with a mixed microbial community. *J. CO2 Utilization* 20, 141–149
34. Bajracharya, S. *et al.* (2017) Bioelectrochemical conversion of CO2 to chemicals: CO2 as next generation feedstock for the electricity-driven bioproduction in batch and continuous mode. *Faraday Discuss.* 202, 433–449
35. Jourdin, L. and Strik, D.P.B.T.B. (2017) Electrodes for cathodic microbial electrosynthesis processes: key-developments and criteria for effective research & implementation. In *Functional Electrodes for Enzymatic and Microbial Bioelectrochemical Systems* (Flexer, V. and Brun, N., eds), pp. 429–473, World Scientific
36. Patil, S.A. *et al.* (2015) A logical data representation framework for electricity-driven bioproduction processes. *Biotechnol. Adv.* 33, 736–744
37. Romans-Casas, M. *et al.* (2023) Selective butyric acid production from CO2 and its upgrade to butanol in microbial electrosynthesis cells. *Environ. Sci. Ecotechnol.* 17, 100303
38. Zhang, F. *et al.* (2013) Fatty acids production from hydrogen and carbon dioxide by mixed culture in the membrane biofilm reactor. *Water Res.* 47, 6122–6129
39. Ammam, F. *et al.* (2016) Effect of tungstate on acetate and ethanol production by the electrosynthetic bacterium *Sporomusa ovata*. *Biotechnol. Biofuels* 9, 163
40. Kantzow, C. *et al.* (2015) Continuous gas fermentation by *Acetobacterium woodii* in a submerged membrane reactor with full cell retention. *J. Biotechnol.* 212, 11–18
41. Roghair, M. *et al.* (2016) Granular sludge formation and characterization in a chain elongation process. *Process Biochem.* 51, 1594–1598
42. Wang, D. *et al.* (2023) Deciphering mixotrophic microbial electrosynthesis with shifting product spectrum by genome-centric metagenomics. *Chem. Eng. J.* 451, 139010
43. Marshall, C. *et al.* (2017) Metabolic reconstruction and modeling microbial electrosynthesis. *Sci. Rep.* 7, 8391
44. Ross, D.E. *et al.* (2017) Metagenome-assembled genome sequences of *Acetobacterium* sp. strain MES1 and *Desulfovibrio* sp. strain MES5 from a cathode-associated acetogenic microbial community. *Genome Announc.* 5, e00938-17
45. Bengelsdorf, F.R. *et al.* (2018) Bacterial anaerobic synthesis gas (Syngas) and CO2+H2 fermentation. *Adv. Appl. Microbiol.* 103, 143–221
46. Litty, D. and Müller, V. (2021) Butyrate production in the acetogen *Eubacterium limosum* is dependent on the carbon and energy source. *Microb. Biotechnol.* 14, 2686–2692
47. Lan, P.T.N. *et al.* (2006) *Bacteroides barnesiae* sp. nov., *Bacteroides salanitronis* sp. nov. and *Bacteroides gallinarum* sp. nov., isolated from chicken caecum. *Int. J. Syst. Evol. Microbiol.* 56, 2853–2859
48. Iino, T. *et al.* (2007) *Oscillibacter valericigenes* gen. nov., sp. nov., a valerate-producing anaerobic bacterium isolated from the alimentary canal of a Japanese corbicula clam. *Int. J. Syst. Evol. Microbiol.* 57, 1840–1845
49. Raes, S.M.T. *et al.* (2017) Continuous long-term bioelectrochemical chain elongation to butyrate. *ChemElectroChem* 4, 386–395

STAR★METHODS

KEY RESOURCES TABLE

Reagent or resource	Source	Identifier
Biological samples		
Mixed microbial culture inoculated in MES reactors	The inoculum was taken from running laboratory MES reactors producing acetate, n-butyrate, and n-caproate from CO_2	N/A
Chemicals, peptides, and recombinant proteins		
NH_4Cl	Across organics	396400010, CAS#7732-18-5
$CaCl_2{\cdot}2H_2O$	Across organics	207780010, CAS#10035-04-8
$MgCl_2{\cdot}6H_2O$	Across organics	413415000, CAS#7791-18-6
KH_2PO_4	Merck Sigma	1.64877.1000, CAS#7778-77-0
Na_2HPO_4	VWR chemicals	28026-292, CAS#7558-79-4
2-bromoethanesulfonic acid	Apollo scientific	BIB1184, CAS#4263-52-9
$FeCl_3{\cdot}6H_2O$	Across organics	21709100, CAS#10025-77-1
H_3BO_3	VWR Lifescience	20185-260, CAS#10043-35-3
$CuSO_4{\cdot}5H_2O$	VWR Lifescience	0330-5006, CAS#7758-99-8
KI	VWR Avantor	8081350, CAS#7681-11-0
$MnCl_2{\cdot}4H_2O$	VWR Avantor	8073890, CAS#13446-34-9
$Na_2MoO_4{\cdot}2H_2O$	Merck Sigma	8.43899.0050, CAS#10102-40-6
$ZnSO_4{\cdot}7H_2O$	Merck Sigma	8078373, CAS#7446-19-7
$CoCl_2{\cdot}6H_2O$	Merck Sigma	8071827, CAS#7791-13-1
$NiCl_2{\cdot}6H_2O$	Merck Sigma	8072500, CAS#7791-20-0
EDTA	Merck Sigma	1.08452.0250, CAS#60-00-4
Deposited data		
Analyzed data	This paper	DOI: 10.4121/28d4cf06-85e2-4c63-a632-179ede79251f
Metagenomic V3-V4 16S rRNA gene Amplicon DNA-sequencing data of cathode microbiome	This paper	NCBI (https://www.ncbi.nlm.nih.gov/) under BioProject accession number PRJNA1071877

METHOD DETAILS

MES reactor setup

Two bioelectrochemical reactors were assembled. Each reactor comprised two identical cathodic and anodic compartments, as well as two supporting plates used to press and close the reactor cell. A scheme of the reactor setup and a picture of the assembled reactor can be seen in Figure 1. Exact reactor dimensions are also given (Figure S9). A biocompatible resin (BioMed Clear Resin V1, Formlabs) and the Form 2 printer (Formlabs) were used to 3D-print all the plates that formed the reactor.

The anode used in this work was a Pt/IrO_2 coated titanium plate (Magneto Special Anodes, Schiedam, The Netherlands). Unmodified carbon felt was used as the cathode electrode material (CTG Carbon GmbH, Germany). Before being used, all felt pieces underwent a cleaning step with 1 mol L^{-1} HCl, 1 mol L^{-1} NaOH, and an UV/ozone treatment as described in Winkelhorst and colleagues [30]. Once in the reactor, the total volume of carbon felt was 9.5 cm^3, with a thickness of 0.5 cm and a total projected surface area of

19 cm^2. In one of the reactors, a titanium wire (Salomon's Metalen, The Netherlands) was placed between two layers of tightly pressed carbon felt (0.25 cm thick each) and used as current collector. The other reactor used an iso-molded graphite plate (GP) (3.2 mm thick, Fuel Cell Store, USA) as current collector, placed parallel to the cathodic plate. Conductive coating (Graphite Conductive Adhesive, Electron Microscopy Sciences, USA) was applied at the surface between current collector and carbon felt in order to enhance the electric connection between both materials [30]. A cation exchange membrane (CEM) (CMI-7000s, Membrane International Inc.) was used to separate the cathodic and anodic compartment.

A pH probe (QP108X, ProSense) was installed in the catholyte recirculation loop outside the reactor and a pH controller (AQUIS touch S, Jumo) was used to control the pH of the catholyte at pH 5.8. pH titrant addition was negligible, likely as a combination of a fairly high phosphate buffer concentration, CO_2 continuous sparging, and proton electrochemical reduction. A bubble column was also installed in the recirculation loop, and used to sparge a CO_2-N_2 mixture into the catholyte. The total volume of the catholyte in the setup was 135 ml. This volume includes the cathodic chamber, recirculation bottle, and all tubing comprising the recirculation loop.

MES reactor operation

The catholyte medium composition was based on the one described in Winkelhorst and coworkers [30], and contained 0.2 g l^{-1} NH_4Cl, 0.015 g l^{-1} $CaCl_2{\cdot}2H_2O$, 0.04 g l^{-1} $MgCl_2{\cdot}6H_2O$, 8.1 g l^{-1} KH_2PO_4, 0.9 g l^{-1} Na_2HPO_4, 1 mL l^{-1} of a trace elements solution, and 4.5 g l^{-1} 2-bromoethanesulfonic acid as methanogenic activity inhibitor. The trace elements solution contained 1.5 g l^{-1} $FeCl_3{\cdot}6H_2O$, 0.15 g l^{-1} H_3BO_3, 0.03 g l^{-1} $CuSO_4{\cdot}5H_2O$, 0.18 g l^{-1} KI, 0.12 g l^{-1} $MnCl_2{\cdot}4H_2O$, 0.06 g l^{-1} $Na_2MoO_4{\cdot}2H_2O$, 0.12 g l^{-1} $ZnSO_4{\cdot}7H_2O$, 0.15 g l^{-1} $CoCl_2{\cdot}6H_2O$, 0.023 g l^{-1} $NiCl_2{\cdot}6H_2O$, and 10 g l^{-1} EDTA. To avoid possible limitations caused by nutrients depletion, a second catholyte medium composition was used from Day 18 containing 0.6 g l^{-1} NH_4Cl, 0.045 g l^{-1} $CaCl_2{\cdot}2H_2O$, 0.12 g l^{-1} $MgCl_2{\cdot}6H_2O$, 8.1 g l^{-1} KH_2PO_4, 0.9 g l^{-1} Na_2HPO_4, 3 mL l^{-1} of a trace elements solution, and 13.5 g l^{-1} 2-bromoethanesulfonic acid. The anolyte composition was identical to the catholyte medium used at that specific moment, without the trace elements solution and the methanogenic inhibitor. The pH of the anolyte was also decreased to 2 with phosphoric acid to facilitate proton crossing over the membrane.

The reactors were operated in continuous mode with a hydraulic retention time (HRT) of 4 days. Both catholyte and anolyte were continuously circulated between the reactor cell and the recirculation bottles at a flow rate of 1.8 l h^{-1}. Dissolved CO_2 was supplied by continuously sparging a gas mixture of CO_2:N_2 50:50 at a rate of 0.1 l min^{-1} in the cathodic bubble column. The volumetric CO_2 mass transfer coefficient (k_La) of the bubble column was determined with the dynamic gassing-out method and found to be 70 h^{-1} (data not shown). The entire setup was placed inside a cabinet, keeping the reactors in the dark to avoid any phototrophic growth. Temperature was kept at 31°C.

The reactors were connected in a three-electrode configuration to a multichannel potentiostat (BioLogic) to control either the cathode potential (chronoamperometry, CA) or the applied current (chronopotentiometry, CP). A 3M Ag/AgCl reference electrode (QM710X, ProSense) was installed in both reactors. The CP reactor was first controlled in potentiostatic mode at -0.85 V vs. SHE (standard hydrogen electrode) from Day 0 to 28, and then switched to galvanostatic mode for the rest of the experiment (Day 248). From Day 28 to 68 a current of -26 A $m^{-1}_{2\ psa}$ was applied, from Day 68 to 114 it was increased to -53 A $m^{-1}_{2\ psa}$, and from Day 114 to the end of the experiment -105 A $m^{-1}_{2\ psa}$ were applied. The CA reactor was controlled at -0.85 V vs. SHE throughout the course of the experiment (221 days).

Each reactor was inoculated on Day 0 with 1.2 g COD_x l^{-1}. The inoculum was taken from running laboratory MES reactors producing acetate, *n*-butyrate, and *n*-caproate from CO_2 [30].

Analytical methods

Twice a week, liquid samples were taken from each reactor. Concentration of C2 to C6 carboxylic acids and alcohols were analyzed by gas chromatography (Thermofisher, USA) using a Stabil-wax™ column with a length of 25 m and internal diameter of 0.2 µm. Colum temperature was kept at 50°C for 7 min, increased to 180°C during 8 min and kept at that temperature for 9 minutes. Helium was used as carrier gas at a flow rate of 1 ml min^{-1} and the ionization detector was kept at 250°C. Production of organics and faradaic efficiency were calculated as described by Raes and colleagues [49]. Biomass-specific growth rates and production rates were calculated as described by Winkelhorst and coworkers [30]. Here, carbon selectivity represents the fraction of carbon going into a

specific product over the total amount of carbon assimilated in all identified products, that is, acetate, butyrate, caproate, and biomass. Datasets used to make the presented figures are available in the online supplemental information.

Samples were filtered with a 0.2 µm microporous filter and their total nitrogen content was analyzed using a TOC analyzer coupled with a TN unit (TOC-L Series Total Organic Carbon Analyzers, Shimadzu, Japan). Oven temperature was kept at 720°C. The optical density of the unfiltered samples was measured at 600 nm with a UV-VIS spectrophotometer (UV-1800 series, Shimadzu, Japan) to account for planktonic cells. To study microbial activity, the method described by Winkelhorst and colleagues [30] was utilized to estimate microbial growth in both biofilm and suspension separately as well as biomass concentration and biomass-specific productivity.

Scanning electron microscopy

Carbon felt pieces were carefully cut at different places along the length of the flow channel (see Figure 6 in the main text). Samples were immediately fixed with 2.5% glutaraldehyde in PBS buffer for 24 h at 4°C, rinsed with PBS buffer and dehydrated with a graded series of ethanol.

DNA extraction and 16S sequence analysis

To extract DNA from the biofilm both on and within the 3D porous cathode, the samples were ground with a pestle in a mortar, periodically incorporating liquid nitrogen to prevent DNA degradation. The resulting powder comprised a mixture of biomass and carbon felt fibers. Subsequently, DNA extraction was carried out using a Qiagen DNeasy PowerBiofilm Kit (Qiagen, Hilden, Germany), employing a detergent lysis method in conjunction with bead beating using an MPTM FastPrep-24 homogenizer (MP Biomedicals, Irvine, CA), following the manufacturer's instructions. The purified DNA underwent quality assessment by measuring the A260/280 and A260/230 ratios (Nanodrop 2000 spectrophotometer (ThermoFischer Scientific, Waltham, MA) and quantification using a Qubit broad-range assay (Qubit 2.0 Fluorometer and Qubit dsDNA BR Assay Kit (ThermoFischer Scientific)).

Microbial community analysis

Microbial community analysis was conducted through 16S rRNA sequencing. For this purpose, extracted DNA samples were sent to Novogene (UK) (Cambridge, UK). The 16S rRNA amplicon was sequenced using barcoded primers 341F (CCTAYGGGRBGCASCAG) and 806R (GGACTACNNGGGTATCTAAT) to amplify regions V3 + V4 of both bacterial and archaeal microorganisms. All polymerase chain reactions (PCR) were carried out in 30 µl reaction volumes, comprising 15 µl of Phusion® High-Fidelity PCR Master Mix (New England Biolabs, Ipswich, MA), 0.2 µM of forward and reverse primers, and approximately 10 ng of template DNA. Thermal cycling involved initial denaturation at 98°C for 10 s, annealing at 50°C for 30 s, elongation at 72°C for 30 s, and a final extension at 72°C for 5 min. PCR products underwent purification through gel electrophoresis using a 2% agarose gel and subsequent extraction using a Qiagen Gel Extraction Kit. Sequencing libraries were generated using the NEBNext® UltraTM DNA Library Prep Kit for Illumina (Illumina, San Diego, CA), following the manufacturer's recommendations, with index codes added. The library quality was evaluated using a Qubit 2.0 Fluorometer (Thermo Scientific) and Agilent Bioanalyzer 2100 system (Agilent, Santa Clara, CA), and the sequencing was performed on an Illumina HiSeq platform to generate 250 bp paired-end reads. Data analysis was performed as described in the supplemental information online.